Water treatment sludge as precursor in non-dehydroxylated kaolin-based alkali-activated cements

J. Mañosa[a], M. Cerezo-Piñas[a], A. Maldonado-Alameda[a], J. Formosa[a], J. Giro-Paloma[a], J.R. Rosell[b], J.M. Chimenos[a,*]

[a] Departament de Ciència de Materials i Química Física, Universitat de Barcelona, C/ Martí i Franquès, 1, Barcelona, 08028, Spain.

[b] Universitat Politècnica de Catalunya (GICITED), Av. Doctor Marañón 44-50, Barcelona, 08028, Spain

* Corresponding author e-mail: chimenos@ub.edu

Abstract

Cement industry production and its materials demand are growing every year, leading to a CO_2 and energy footprint increase. The drinking water production is increasing in water treatment plants due to the population growth, raising in turn the waste materials produced. Since these wastes are mainly managed in landfills, this preliminary research work is focused on providing a new sustainable option for valorisation processes, based on the environmental demand of the cement industry. Alkali-activated cements (AACs) can become a proper option to give the water treatment sludge a new life cycle, as they can compete with ordinary Portland cement (OPC) both in properties and sustainability. The main purpose of this study was to evaluate and formulate different AACs based on the use of both raw clay and the water treatment sludge (WTS), as precursors. The raw clay was used without previous thermal dehydroxylation treatment, and the WTS, an aluminosilicate-rich waste, was used partially replacing the raw clay in the AACs formulations. Both precursors and the formulated AACs were characterized by X-ray diffraction (XRD), X-ray fluorescence (XRF) and Fourier-transformed infrared spectroscopy (FT-IR). In addition, the compressive strength, the chemical stability (hydrolytic degradation), and the environmental impact for each AACs formulation were also determined. The results showed that AACs specimens formulated with 20 wt.% of WTS (replacing the raw clay) provided the best results, considering both compressive strength and resistance to hydrolytic degradation. Then, it is possible to formulate AACs using raw clay, without prior thermal dehydroxylation treatment, and WTS as precursors.

Keywords: Alkali-activated materials; geopolymers; water treatment sludge; raw clay.

1. Introduction

Ordinary Portland cement (OPC) is produced in more than 150 countries across the globe, where over half of the world's cement is currently produced in China. During 2018, the global production capacity of cement was approximately 4,100 Mt (Reilly, 2019). The OPC industry is one of the most energy consuming sector, (12 to 15% of industrial energy) and one of the most contributors to CO_2 emissions 6 to 8% of the global carbon emissions) (Andrew, 2017; Shen et al., 2017). This is due to the huge amount of cement produced and the thermal processes used in its manufacture. In Spain, the cement industry consumes around 3 Mt per year of fossil fuel, releasing 18 Mt of CO_2 to the atmosphere, representing the 7% of the total CO_2 national emissions (García-Gusano et al., 2015).

In order to achieve proper sustainable production, cement manufacturers are trying to decrease both emissions and energy consumption. To reach this goal, the industry is decreasing the usage of the primary material and it is increasing the renewable resources use. Besides, according to a circular economy model (Hossain et al., 2017), it is giving a new productive life to some waste materials. This circular model involves the reusing and recycling end-of-life materials and products criteria, extending their life cycle. Thus, it increased the use of waste as secondary resources for new materials development. Alkali-activated materials (AAMs), and especially the alkali-activated cements (AACs), turn up as a feasible binder's solution to OPC. AACs have low energy consumption during its processing and the reuse of industrial waste or by-products formulations as precursors contributes to the greenhouse gas (GHG) emissions savings (Duxson and Provis, 2008; Provis and Bernal, 2014).

A wide range of alumina- and silica-containing industrial waste has been used as precursors in AAMs formulations. Some examples considering both low- and high-calcium

content in AAMs are metallurgical slags, power plant fly ashes, municipal solid waste incineration bottom ash (Duxson et al., 2007; Provis and Bernal, 2014; Wongsa et al., 2017; Provis, 2018; Maldonado-Alameda et al., 2020), etc. Moreover, abundant natural resources can also be employed as AAMs precursors, like clay or clay-based minerals (Ruiz-Santaquiteria et al., 2013; Liew et al., 2016; Zhang et al., 2020c). The selection of the optimal precursor depends on the local availability of suitable raw materials (Provis, 2018). Clay and clay-based materials, that are abundant through the Earth's crust, could be potential precursors for AACs formulations. However, due to the low reactivity of clays, their usage as precursor requires previous dehydroxylation thermal treatment (between 500ºC and 850ºC), which depends on the clay and the aluminosilicate structural layer stacking order (Seiffarth et al., 2013; Belmokhtar et al., 2018; Bouna et al., 2020; Haw et al., 2020). Dehydroxylated disordered clay shows higher pozzolanic activity than the starting materials (e.g. metakaolin from kaolinite). The thermal process transforms the crystalline phases into metastable phases, increasing the SiO_2 and Al_2O_3 availability, which are the required compounds for the formation of previous forming gels (N-A-S-H). It should be noted that this thermal treatment implies an additional energetic and economic cost, entailing a low sustainable AACs synthesis and environment footprint.

The chemical and/or mechanical activation of clays (e.g. kaolinitic clay), without prior dehydroxylation heating treatment, was studied elsewhere with promising results (Mackenzie, 2009; Slaty et al., 2013; Hounsi et al., 2014; Esaifan et al., 2015; Zhang et al., 2020a, 2020b). Although the SiO_2/Al_2O_3 availability was not as large as in the dehydroxylated clay, chemical and/or mechanical treatments allow obtaining AACs, usually

mortars using silica sand as filler, with good performance for its use as a construction material.

On the other hand, drinking water consumption is increasing steadily due to population growth and the need to supply tap water with the health guarantees required for human health (Rodríguez et al., 2010). The drinking water supply requires proper treatment of continental water (surface water), which is performed in the water treatment plants (WTP). During the surface water treatment process, i.e. coagulation-flocculation, sedimentation, filtration and disinfection (Ahmad et al., 2016), a large volume of water treatment sludge (WTS) is generated. In this regard, it is estimated that a typical WTP produces about 100 kt of WTS per year (Bourgeois et al., 2004). The WTS is a clay-based waste mainly formed by suspended sediments carried by the surface waters, which are aluminosilicates rich materials, precipitates formed during the treatment process, and traces of unreacted chemicals. Most of the WTS is collected in the coagulation-flocculation step, where the use of aluminium-based agents is usual. WTS is mainly disposed of in landfills (Cremades et al., 2018; De Carvalho Gomes et al., 2019), as its use is not regulated yet. Consequently, the need to find a new destination for these sludge wastes has arisen, where the ceramic and cement industries are some of the most promising targets (Cremades et al., 2018; Godoy et al., 2019).

The main goal of this study was to evaluate the potential of new AACs binders formulated with WTS, partially replacing a commercial raw clay commonly used in the ceramic industry. To increase sustainability and applicability, this preliminary research work was focused on the use of both precursors without prior thermal activation and using alkali-activators in the formulation of the AACs. The use of common non-dehydroxylated clay and a clay-based waste with higher available aluminium content in the formulation of AACs contributes to the

development of alternative sustainable binder materials and provides an important added value to the WTS.

2. Materials and methods

2.1. Materials

A commercial raw clay supplied by the Argiles Colades S.A. company (Girona, Spain) was used as precursor in the different AACs formulations. The same natural raw clay was used as a binder for the formulation of alkali-activated mortars, using silica sand as filler, in previous research work, with promising results (Calderón, 2019). In the above-mentioned cited study the clay was not thermally dehydroxylated, its activation was carried out by means of an alkali solution of $Na(OH)/Na_2SiO_3$.

WTS used in this research was supplied by Aigües del Ter Llobregat (ATL) company from the WTP located in Abrera (Barcelona, Spain). This treatment plant manages the upstream water supply for the metropolitan area of Barcelona (Spain). Currently, as far as it is known, the WTS generated in this plant is not reused and it is managed as non-hazardous waste in landfills.

Sodium hydroxide (NaOH) in the form of 98.5% pure pellets (Labkem) was used as the activator in the AACs formulations. It was dissolved in deionized water to obtain the different molarity (M) dissolutions used in the experimental trials (2M, 4M, 8M, 10M, and 12M).

2.2. Experimental procedure

Activation of a non-dehydroxylated clay by the addition of NaOH and/or sodium silicate activating solutions has already been addressed (Calderón, 2019; Emmanuel et al., 2019; Marsh et al., 2019). However, in this preliminary study, only the use of NaOH solutions as

activators has been considered. Prior to the preparation of the different AACs formulations, the proper concentration of the NaOH activator solution and the optimal L/S ratio were determined. The L/S ratio is referred between the activator solution (attributed to the liquid, L) and the precursor (specified as solid, S). The availability of SiO_2 and Al_2O_3 as reactive phases for both precursors were determined through chemical attacks with NaOH solutions (2M, 4M, 8M, 10M, and 12M). For these experimental trials, 1g of each precursor was mixed with 100 mL of each different molarity solution and stirred constantly for 5 h at 80 ºC in a sealed plastic container (Ruiz-Santaquiteria et al., 2011). The resulting solution was filtered and analysed per duplicate through inductively coupled plasma optical emission spectrometry (ICP-OES), using Perkin Elmer Optima ICP-OES 3200 RL equipment. It was quantified the Si and Al leached. From the availability of both elements, the proper concentration (M) of the activator solution was determined.

Different formulations were carried out (Table 1) to assess the effect of partially replacing WTS as precursor in the AACs formulations. Six cubic shape specimens (25x25x25 mm) were prepared (Fig. 1) for each formulation. L/S ratio was fixed for minimum workability found in previous tests with the best mechanical resistance. The L/S ratio was 0.6 except for the case of WTS-80 because of the lack of workability, where the ratio was 0.75. After formulating and moulding the pastes, the moulds were placed into a closed plastic bag and set in a stove at constant temperature (80 ºC) for 24 h (Calderón, 2019). Subsequently, the moulds were removed from the stove and cooled at room temperature. Afterwards, specimens were demoulded and stored for 14 days at room temperature before testing.

At 14 days of curing one specimen of each AACs formulation was milled to determine the neoformed mineral phases and to evaluate the most representative functional groups,

through XRD and Fourier-transform infrared spectroscopy (FT-IR) techniques, respectively. FT-IR spectra were acquired in attenuated total reflectance mode (ATR) in the range 4000 - 450 cm^{-1}, with a resolution of 4 cm^{-1}, using a Spectrum Two™ Perkin Elmer spectrometer.

2.3. Mechanical and chemical tests

Mechanical properties were tested through compressive strength (σ_c) for each AACs formulated. The σ_c tests after 14 curing days were performed per triplicate following the UNE-EN 196-1 standard, using a universal testing machine Incotecnic MULTI-R1, equipped with 20 kN load cell. A progressive load until fracture was applied with a loading rate of 240 $kg \cdot s^{-1}$.

The chemical stability of the cured AACs was evaluated introducing the cubic (25x25x25 mm) specimens of each formulation in boiling water for 20 min (Davidovits, 2008; Zhu et al., 2018). Afterwards, the specimens remained at room temperature until constant weight in a desiccator with silica gel. Before and after the chemical stability tests, the samples were weighed to determine the mass loss and to verify the chemical stability and resistance to the specimens' dissolution. If the sample was still whole or with a weight loss of less than 10%, the chemical stability was considered adequate and the test was considered a success.

Finally, to assess the environmental impact and to evaluate the hazardousness of the AACs formulated with WTS as precursor, the leaching potential of heavy metals and metalloids were studied. Leaching tests in deionised water for 24 h were conducted according to the European standard (EN 12547-4). PerkinElmer ELAN 6000 ICP mass spectrometry (ICP-MS) device was used to analyse some heavy metal(loid)s in the obtained eluates (As, Ba, Cd, Cr, Cu, Hg, Mo, Pb, Ni, Se, Sb, and Zn).

3. Results and discussion

3.1. Precursors' composition

Table 2 shows the chemical composition of the dry clay (105ºC overnight). It was determined by X-ray fluorescence (XRF), using a Philips PW2400 X-ray sequential spectrophotometer. As expected, the major compounds were SiO_2 (59.9 wt.% of clay) and Al_2O_3 (22.9 wt.% of clay). The X-ray diffraction (XRD) pattern of the clay, using a Bragg-Brentano Siemens D-500 powder diffractometer with CuK α-radiation, showed kaolinite and quartz as the main crystalline mineral phases. The presence of hematite, calcite, muscovite, and halloysite was also identified. Particle size distribution, determined with a laser analyser Beckman Coulter® LSTM 13 320, showed a narrow distribution, with 50% of particles (d_{50}) below 21.58 μm and 90% of particles (d_{90}) below 52.52 μm.

Chemical composition of WTS, determined by XRF, is shown in Table 2. As expected, the major compounds of the sludge were SiO_2 and Al_2O_3, although the CaO content was also significant. It is important to highlight the high value of loss of ignition (LOI, Table 2) of the WTS sample. According to the results obtained by thermogravimetric analysis (TGA, Fig. 2), using an SDT Q600 device from TA Instruments in an air atmosphere (50 $mL \cdot min^{-1}$) with a heating rate of 10 $ºC \cdot min^{-1}$ up to 1,000 ºC, the LOI result obtained in Table 2 can be attributed to the presence of adsorbed water (2.20 wt. %), molecularly-bound water (5.21 wt. %), hydroxides (11.66 wt.% of WTS), organic matter (3.46 wt.% of WTS) and a high content of carbonates (13.39 wt.% of WTS).

The XRD pattern of the WTS showed quartz, illite and muscovite as main crystalline mineral phases. Dolomite, calcite, and hematite were also identified. The particle size distribution of WTS showed a d_{50} of 45.24 μm and a fraction d_{90} lower than 227.5 μm.

Previously to the AACs formulations, the whole WTS sample was sieved up to 80 μm, and the fraction coarser than 80 μm was milled and sieved again. Therefore, all the WTS particles must be below 80 μm.

3.2. Alkali-activation products

The availability of both gel-forming compounds of the SiO_2 and Al_2O_3 cementing phases, resulting from the chemical attacks with different molarities of NaOH solutions, are shown in Fig. 3 for both precursors, clay and WTS.

As can be seen in Fig. 3 (a, b) approximately 18 wt.% of the SiO_2 content and 36 wt.% of the Al_2O_3 content was activated by the alkali attack, despite the clay was not thermally activated. As expected, the activation of clay through an alkali reaction is much less than the activation carried out from a previously thermally dehydroxylated clay (Emmanuel et al., 2019). Moreover, considering the 8M, 10M, and 12M, the SiO_2/Al_2O_3 molar ratio was very close to 2.00 (2.32 - 1.92), which is considered the proper molar ratio to form AACs (Duxson et al., 2005). In contrast, as it is shown in Fig. 3 (c, d) the alkali activation from the WTS was significantly lower than the obtained from the clay. While the availability of SiO_2 in WTS increased when the concentration of the alkali solution increased, the availability of Al_2O_3 did not vary significantly. The maximum activation in WTS of SiO_2 was 10 wt.% of the SiO_2 contained in the precursor, using a 12M NaOH solution, while the activation of Al_2O_3 ranged between 16 to 20 wt.%. It is surprising that, although the Al_2O_3 content was lower than the SiO_2 content as showed in Table 1, the activation of Al_2O_3 was greater than the SiO_2 one. This fact can be attributed to the presence of amorphous phase contained in the WTS, consisting mainly of amorphous $Al(OH)_3$ gels generated from the products added in the coagulation-flocculation processes.

Regarding the results of the chemical attacks above described, it was considered to use the 10M NaOH solution as the proper activate solution for all the AACs studied formulations (Table 2). Furthermore, an excess of activator (e.g. 12M NaOH) induced to efflorescence of unreacted sodium and the formation of a sodium carbonate coating on the samples' surface (see bottom row in Fig. 1).

XRD diffractograms of WTS-0 and WTS-20 samples are shown in Fig. 4. XRD patterns for the different percentages of WTS partially replacing clay were similar to each other and resembled that of the WTS-0. As can be seen, the major crystalline phases in both alkali-activated samples were quartz, kaolinite and muscovite. These mineral phases come from the unreacted raw clay used as precursor. Note that halloysite determined in the raw clay was not detected in the alkali-activated samples. Moreover, the weakening of the diffraction peaks of kaolinite suggests that this mineral phase might also have participated in the alkali-activation reactions. After alkali activation, several phases appeared as a result of the reaction, attributed to sodium aluminium silicate hydrate and phillipsite, this last belonging to the zeolite group. Sodium carbonate was also identified. It should be noted that small peaks of calcium silicate hydrate (C-S-H) in the XRD diffractogram of WTS-20 were also identified (see upper right of Fig. 4), which involves the calcium in the gelation process of alkali-activated formulations where WTS was also used as precursor. In addition, the reddish tone of the raw clay due to hematite was drastically reduced when this mineral phase disappeared, and the iron was incorporated in the neoformed phases.

FT-IR spectra for both clay and WTS precursors before the alkali activation are shown in Fig. 5. The bands at 3693 cm^{-1}, 3622 cm^{-1} were attributed to OH^- stretching and the band at 1645 cm^{-1} to OH^- bending vibrations (El Hafid and Hajjaji, 2015). In the midwavenumber

region, the peaks at 1115 cm^{-1}, 792 cm^{-1}, and 749 cm^{-1} were associated to Si-O-Si symmetrical stretching (Heah et al., 2012), which vanished during alkali activation. The main peaks at 1027 cm^{-1} and 997 – 1000 cm^{-1} were assigned to Si-O-T (T=Si, Al) asymmetric stretching vibration. The displacement of these last bands to lower wavenumbers, affecting the Al-O and Si-O bonds, can be related to the formation of AACs (El Hafid et al., 2017). The band at 912 cm^{-1} was attributed to Al-OH bending mode (Puligilla and Mondal, 2015). Unlike the clay, the WTS spectrum also showed two other peaks at 1430 cm^{-1} and 875 cm^{-1}. These were associated to O-C-O bonds (El Hafid et al., 2017), indicating the presence of carbonates in the sludge (dolomite and calcite), as previously determined by XRD.

Fig. 6 shows the FT-IR spectra of clay before and after alkali-activation (WTS-0). The peaks of the clay corresponding to Si-O-T asymmetric stretching were shifted to a lower frequency, which was around 965 cm^{-1}, as well as the fading of other bands described previously in the FT-IR of the precursor. Moreover, the broadband at 1490 – 1300 cm^{-1} was associated to the O-C-O bonds, indicating a certain amount of sodium carbonates formed by the atmospheric CO_2 adsorption at high alkali pH (El Hafid et al., 2017; Gao et al., 2017; Belmokhtar et al., 2018).

The FT-IR midwavenumber region spectra of the AACs specimens formulated with WTS as precursor, replacing different percentages of clay (0, 5, 10, and 20 wt.%), are shown in Fig. 7. Increasing WTS percentage, the main peak at 965-979 cm^{-1} shifts to higher frequencies. This broadband is actually due to the contribution of multiple bands which are overlapped (El Hafid et al., 2017; Belmokhtar et al., 2018). These displacements could initially be attributed to a higher contribution of Si-O-T (T = Si, Al) asymmetric stretching vibration, due to a greater addition of the WTS as precursor. However, these shifts could also

indicate changes in the AACs structures, possibly due to the participation of calcium in the gelation and the formation of calcium silicate hydrate gel, both C-S-H and C-(N)-A-S-H gels (García-Lodeiro et al., 2008).

To clarify and reveal the overlap of the fundamental band, the deconvolution of the FT-IR spectra in the midwavenumber region (1100 – 850 cm^{-1}) is shown in Fig. 8. Gaussian functions were added to adjust the shape of the spectra. The deconvoluted band of raw clay (Fig. 8a) showed the presence of bands at 1028 cm^{-1}, 999 cm^{-1}, and 986 cm^{-1}, which were assigned to Si-O-T (Si, Al) stretching vibrations (El Hafid and Hajjaji, 2015), and two peaks at 933 cm^{-1} and 909 cm^{-1}, both corresponding to Al_2-OH bending vibrations (Tironi et al., 2012; Tămăşan et al., 2013; El Hafid and Hajjaji, 2015). The deconvoluted band of the alkali-activated specimens (Fig. 8b-e) showed the same peaks at 1029 - 1026 cm^{-1}, 996 - 999 cm^{-1} and 911 cm^{-1}, also determined in the deconvolution of clay (Fig. 8a). These peaks were attributed to vibrations of the unreacted clay. Note that the contribution of these non-shifted peaks to the fitted curve decreases significantly in the alkaline activated samples. In contrast, the peak at 986 cm^{-1} (Fig. 8a) was shifted to lower wavenumber (964 cm^{-1}) and increased its contribution to the fitted curve in the alkali-activated clay (WTS-0, Fig. 8b), as a consequence of the polymerization of the raw clay and the formation of N-A-S-H gel. Subsequently, as the percentage of WTS replacing clay increases, this peak shifts again towards higher frequencies (970 - 976 cm^{-1}, Fig. 8c-e). This behaviour can also be observed in the shift of the peak at 933 - 934 cm^{-1} towards higher wavenumbers (936 - 950 cm^{-1}, Fig. 8c-e). These displacements are attributed to the increased availability of aluminium and calcium from WTS, as well as the formation of both C-S-H and C-A-S-H gels (García-Lodeiro et al., 2008).

3.3. Mechanical strength

Fig. 9 presents the variation of compressive strength (σc) as a function of WTS percentage in the AACs formulation. The obtained results were in agreement with the published elsewhere by using non-dehydroxylated kaolin (Heah et al., 2012). From WTS-0 to WTS-5, a slight σ_c decrease from 2.4 MPa to 2.2 MPa can be noticed. After 5 wt.%, the σ_c increased with the percentage of WTS added, reaching a maximum of 3.4 MPa with the 20 wt.% of WTS addition. Subsequently, the tendency began to decrease as the addition of WTS increased. Heah et al. (Heah et al., 2012) attributed the differences found in the σ_c of geopolymers formulated with non-dehydroxylated kaolin to the variations in the SiO_2/Al_2O_3, SiO_2/Na_2O, and Al_2O_3/Na_2O molar ratios. In this assumption, given the poor reactivity of both clay and WTS (see Fig. 3), it is expected that the SiO_2/Na_2O and Al_2O_3/Na_2O molar ratios would be very low in all the AACs formulated. This fact justifies the low compressive strength results obtained. Only the calcium contribution in the formation of gels, giving C-S-H and C-(N)-A-S-H type gels structures, can justify the slight increase in compressive strength for some formulations, as some authors suggested (Provis, 2014). It should be noted that the formulation offering the greatest resistance to hydrolytic degradation (20 wt.% of WTS, see Table 3) was also the one exhibiting the greatest compressive strength. This shows the structural cohesion of the cementitious phase.

3.4. Chemical stability

Table 3 shows the chemical stability tests results for the different AACs, where three formulations succeed in boiling water. Both specimens formulated with 0 wt.% and 80 wt.% of WTS failed during the tests, collapsing their structure. In these cases, the expected network was not formed, and the main cementitious phase, probably dry water glass (Na_2SiO_3), was not stable and consistent enough under the tests conditions. Furthermore, although the

297 specimen formulated with 40 wt.% of WTS as precursor passed the tests, the sample lost
298 more than 10 % of its mass and was therefore considered failed. This mass loss was enough
299 to affect the structural consistency of the binder. Hence, three formulations presented the
300 expected integrity, showing that these AACs formulations resisted to hydrolytic degradation
301 and maintained the structural cohesion. This fact indicates the binder phases were not due to
302 the water glass drying but rather to the alkali activation of the precursors.

303 3.5. Environmental behaviour

304 Leaching tests for granular waste materials were performed to assess the potential
305 environmental impact of the AACs formulated using waste as precursor. The standard
306 leaching test EN 12457-4 was conducted for the three AACs formulation that did not show
307 the hydrolytic degradation (see Table 3), and the mean results of the duplicates are shown in
308 Table 4. The leaching tests results for both precursors (clay and WTS) and the limits and
309 criteria of non-hazardous and hazardous waste are also presented in Table 4.

310 In general, from Table 4 can be seen that the concentrations of heavy metals and
311 metalloids in leachates obtained for both precursors and the three AACs formulations were
312 below the limits established for their classification as non-hazardous waste. Most of the
313 metal(loid)s studied are below the threshold for classification as inert material. Only Cr and
314 As slightly exceed the limit of inert, being well below the threshold of non-hazardous waste.
315 Note the slight increase of the metal(loid)s concentrations in leachates generated from the
316 AACs, compared to the raw materials used in their formulations. This fact is due to the high
317 alkali pH and therefore, the strong precursor activation. The small differences between the
318 AACs formulations were more likely due to the heterogeneity of clay and WTS than
319 differences between AACs formulations.

4. Conclusions

The possibility of formulating AACs using a commercial raw clay as precursor without prior thermal dehydroxylation treatment has been studied. Partial substitutions of raw clay for WTS have been performed to provide an added value to this waste. AACs with WTS content up to 80 wt.% were formulated and their properties were characterised. The following conclusions must be highlighted:

- The addition of WTS affected the properties of the AACs, adding Al_2O_3 and CaO, promoting the formation of C-S-H and C-A-S-H gels.
- The availability of SiO_2 and Al_2O_3 for both precursors was low, hence most of the precursors remained unreacted, and the amount of newly formed binder phases was low.
- Low compressive strengths were obtained for the AACs, similar to other non-dehydroxylated clay-based AACs.
- The optimal formulation was reached by adding 20 wt.% of WTS. The AACs presented the maximum content of C-S-H and C-A-S-H gels, the highest compressive strengths and the best chemical stability.
- The effect of WTS addition to the environmental impact was negligible. The contents of heavy metals and metalloids were well below the limits for non-hazardous materials for all AACs and precursors.

Funding

The work is partially funded by the Spanish Government (BIA2017-83912-C2-1-R).

Acknowledgements

The authors would like to thank the Catalan Government for the quality accreditation given to the DIOPMA research group (2017 SGR 118). The authors also want to thank SORIGUÉ and NORDVERT S.L. for providing access to sampling sites. Mr Alex Maldonado-Alameda and Mr Jofre Mañosa are grateful to the Catalan Government for their research Grants, FI-DGR 2017 and FI 2020, respectively. Dr Jessica Giro-Paloma is a Serra Húnter Fellow.

References

Ahmad, T., Ahmad, K., Alam, M., 2016. Characterization of Water Treatment Plant's Sludge and its Safe Disposal Options. Procedia Environmental Sciences 35, 950–955. https://doi.org/10.1016/J.PROENV.2016.07.088

Andrew, R.M., 2017. Global CO_2 emissions from cement production. Earth System Science Data 1–52.

Belmokhtar, N., El Ayadi, H., Ammari, M., Ben Allal, L., 2018. Effect of structural and textural properties of a ceramic industrial sludge and kaolin on the hardened geopolymer properties. Applied Clay Science 162, 1–9. https://doi.org/https://doi.org/10.1016/j.clay.2018.05.029

Bouna, L., Ait El Fakir, A., Benlhachemi, A., Draoui, K., Ezahri, M., Bakiz, B., Villain, S., Guinneton, F., Elalem, N., 2020. Synthesis and characterization of mesoporous geopolymer based on Moroccan kaolinite rich clay. Applied Clay Science 196, 105764. https://doi.org/https://doi.org/10.1016/j.clay.2020.105764

Bourgeois, J.C., Walsh, M.E., Gagnon, G.A., 2004. Treatment of drinking water residuals: Comparing sedimentation and dissolved air flotation performance with optimal cation ratios. Water Research 38, 1173–1182. https://doi.org/10.1016/j.watres.2003.11.018

Calderón, J.C., 2019. Estudio experimental de geopolímeros de arcillas (Experimental study of clay geopolymers). Universitat Politécnica de Catalunya.

Cremades, L. V, Cusidó, J.A., Arteaga, F., 2018. Recycling of sludge from drinking water treatment as ceramic material for the manufacture of tiles. Journal of Cleaner Production 201, 1071–1080. https://doi.org/https://doi.org/10.1016/j.jclepro.2018.08.094

Davidovits, J., 2008. Geopolymer Chemistry and Applications.

De Carvalho Gomes, S., Zhou, J.L., Li, W., Long, G., 2019. Progress in manufacture and properties of construction materials incorporating water treatment sludge: A review. Resources, Conservation and Recycling 145, 148–159. https://doi.org/10.1016/j.resconrec.2019.02.032

Duxson, P., Fernández-Jiménez, A., Provis, J.L., Lukey, G.C., Palomo, A., Van Deventer, J.S.J., 2007. Geopolymer technology: The current state of the art. Journal of Materials Science 42, 2917–2933. https://doi.org/10.1007/s10853-006-0637-z

Duxson, P., Provis, J.L., 2008. Designing Precursors for Geopolymer Cements. Journal of the American Ceramic Society 91, 3864–3869. https://doi.org/10.1111/j.1551-2916.2008.02787.x

Duxson, P., Provis, J.L., Lukey, G.C., Mallicoat, S.W., Kriven, W.M., van Deventer, J.S.J., 2005. Understanding the relationship between geopolymer composition, microstructure and mechanical properties. Colloids and Surfaces A: Physicochemical and Engineering Aspects 269, 47–58. https://doi.org/https://doi.org/10.1016/j.colsurfa.2005.06.060

El Hafid, K., Hajjaji, M., 2015. Effects of the experimental factors on the microstructure and the properties of cured alkali-activated heated clay. Applied Clay Science 116–117, 202–210. https://doi.org/https://doi.org/10.1016/j.clay.2015.03.015

El Hafid, K., Hajjaji, M., El Hafid, H., 2017. Influence of NaOH concentration on microstructure and properties of cured alkali-activated calcined clay. Journal of Building Engineering 11, 158–165. https://doi.org/https://doi.org/10.1016/j.jobe.2017.04.012

Emmanuel, E., Paris, M., Deneele, D., 2019. Insights on the clay reactivity in alkaline media: Beyond filler role for kaolin. Applied Clay Science 181, 105210. https://doi.org/https://doi.org/10.1016/j.clay.2019.105210

Esaifan, M., Rahier, H., Barhoum, A., Khoury, H., Hourani, M., Wastiels, J., 2015. Development of inorganic polymer by alkali-activation of untreated kaolinitic clay: Reaction stoichiometry, strength and dimensional stability. Construction and Building Materials 91, 251–259. https://doi.org/https://doi.org/10.1016/j.conbuildmat.2015.04.034

Gao, X., Yuan, B., Yu, Q.L., Brouwers, H.J.H., 2017. Characterization and application of municipal solid waste incineration (MSWI) bottom ash and waste granite powder in alkali activated slag. Journal of Cleaner Production 164, 410–419. https://doi.org/https://doi.org/10.1016/j.jclepro.2017.06.218

García-Gusano, D., Garraín, D., Herrera, I., Cabal, H., Lechón, Y., 2015. Life Cycle Assessment of applying CO2 post-combustion capture to the Spanish cement production. Journal of Cleaner Production 104, 328–338. https://doi.org/10.1016/J.JCLEPRO.2013.11.056

García-Lodeiro, I., Fernández-Jiménez, A., Blanco, M.T., Palomo, A., 2008. FTIR study of the sol-gel synthesis of cementitious gels: C-S-H and N-A-S-H. Journal of Sol-Gel Science and Technology 45, 63–72. https://doi.org/10.1007/s10971-007-1643-6

Godoy, L.G.G. de, Rohden, A.B., Garcez, M.R., Costa, E.B. da, Da Dalt, S., Andrade, J.J. de O., 2019. Valorization of water treatment sludge waste by application as supplementary cementitious material. Construction and Building Materials 223, 939–950. https://doi.org/10.1016/j.conbuildmat.2019.07.333

Haw, T.T., Hart, F., Rashidi, A., Pasbakhsh, P., 2020. Sustainable cementitious composites reinforced with metakaolin and halloysite nanotubes for construction and building applications. Applied Clay Science 188, 105533. https://doi.org/https://doi.org/10.1016/j.clay.2020.105533

Heah, C.Y., Kamarudin, H., Mustafa Al Bakri, A.M., Bnhussain, M., Luqman, M., Khairul Nizar, I., Ruzaidi, C.M., Liew, Y.M., 2012. Study on solids-to-liquid and alkaline activator ratios on kaolin-based geopolymers. Construction and Building Materials 35, 912–922. https://doi.org/https://doi.org/10.1016/j.conbuildmat.2012.04.102

Hossain, M.U., Poon, C.S., Lo, I.M.C., Cheng, J.C.P., 2017. Comparative LCA on using waste materials in the cement industry: A Hong Kong case study. Resources, Conservation and Recycling 120, 199–208. https://doi.org/10.1016/j.resconrec.2016.12.012

Hounsi, A.D., Lecomte-Nana, G., Djétéli, G., Blanchart, P., Alowanou, D., Kpelou, P., Napo, K., Tchangbédji, G., Praisler, M., 2014. How does Na, K alkali metal concentration change the early age structural characteristic of kaolin-based geopolymers. Ceramics International 40, 8953–8962. https://doi.org/https://doi.org/10.1016/j.ceramint.2014.02.052

Liew, Y.-M., Heah, C.-Y., Mohd Mustafa, A.B., Kamarudin, H., 2016. Structure and properties of clay-based geopolymer cements: A review. Progress in Materials Science 83, 595–629. https://doi.org/https://doi.org/10.1016/j.pmatsci.2016.08.002

Mackenzie, K.J.D., 2009. 14 - Utilisation of non-thermally activated clays in the production of geopolymers, in: Provis, J.L., van Deventer, J.S.J.B.T.-G. (Eds.), Woodhead Publishing Series in Civil and Structural Engineering. Woodhead Publishing, pp. 294–314. https://doi.org/https://doi.org/10.1533/9781845696382.2.294

Maldonado-Alameda, A., Giro-Paloma, J., Svobodova-Sedlackova, A., Formosa, J., Chimenos, J.M., 2020. Municipal solid waste incineration bottom ash as alkali-activated cement precursor depending on particle size. Journal of Cleaner Production 242, 118443. https://doi.org/10.1016/j.jclepro.2019.118443

Marsh, A., Heath, A., Patureau, P., Evernden, M., Walker, P., 2019. Phase formation behaviour in alkali activation of clay mixtures. Applied Clay Science 175, 10–21. https://doi.org/https://doi.org/10.1016/j.clay.2019.03.037

Provis, J.L., 2018. Alkali-activated materials. Cement and Concrete Research 114, 40–48. https://doi.org/https://doi.org/10.1016/j.cemconres.2017.02.009

Provis, J.L., 2014. Geopolymers and other alkali activated materials: why, how, and what? Materials and Structures 47, 11–25. https://doi.org/10.1617/s11527-013-0211-5

Provis, J.L., Bernal, S.A., 2014. Geopolymers and Related Alkali-Activated Materials. Annual Review of Materials Research 44, 299–327. https://doi.org/10.1146/annurev-matsci-070813-113515

Puligilla, S., Mondal, P., 2015. Co-existence of aluminosilicate and calcium silicate gel characterized through selective dissolution and FTIR spectral subtraction. Cement and

Concrete Research 70, 39–49. https://doi.org/https://doi.org/10.1016/j.cemconres.2015.01.006

Reilly, J.F., 2019. Mineral Commodity Summaries 2019. Reston, Virginia, USA.

Rodríguez, N.H., Ramírez, S.M., Varela, M.T.B., Guillem, M., Puig, J., Larrotcha, E., Flores, J., 2010. Re-use of drinking water treatment plant (DWTP) sludge: Characterization and technological behaviour of cement mortars with atomized sludge additions. Cement and Concrete Research 40, 778–786. https://doi.org/10.1016/j.cemconres.2009.11.012

Ruiz-Santaquiteria, C., Fernándes-Jiménez, a, Palomo, a, 2011. Quantitative determination of reactive SiO2 and Al2O3 in aluminosilicate materials. 13th International Congress on the Chemistry of Cement. 1–7.

Ruiz-Santaquiteria, C., Fernández-Jiménez, A., Skibsted, J., Palomo, A., 2013. Clay reactivity: Production of alkali activated cements. Applied Clay Science 73. https://doi.org/10.1016/j.clay.2012.10.012

Seiffarth, T., Hohmann, M., Posern, K., Kaps, C., 2013. Effect of thermal pre-treatment conditions of common clays on the performance of clay-based geopolymeric binders. Applied Clay Science 73, 35–41. https://doi.org/https://doi.org/10.1016/j.clay.2012.09.010

Shen, W., Liu, Y., Yan, B., Wang, J., He, P., Zhou, C., Huo, X., Zhang, W., Xu, G., 2017. Cement industry of China: Driving force, environment impact and sustainable development. Renewable and Sustainable Energy Reviews 75, 618–628. https://doi.org/10.1016/j.rser.2016.11.033

Slaty, F., Khoury, H., Wastiels, J., Rahier, H., 2013. Characterization of alkali activated kaolinitic clay. Applied Clay Science 75–76, 120–125. https://doi.org/https://doi.org/10.1016/j.clay.2013.02.005

Tămăşan, M., Radu, T., Simon, V., 2013. Spectroscopic characterisation and in vitro behaviour of kaolinite polyvinyl alcohol nanocomposite. Applied Clay Science 72, 147–154. https://doi.org/https://doi.org/10.1016/j.clay.2012.11.009

Tironi, A., Trezza, M.A., Irassar, E.F., Scian, A.N., 2012. Thermal Treatment of Kaolin: Effect on the Pozzolanic Activity. Procedia Materials Science 1, 343–350. https://doi.org/https://doi.org/10.1016/j.mspro.2012.06.046

Wongsa, A., Boonserm, K., Waisurasingha, C., Sata, V., Chindaprasirt, P., 2017. Use of municipal solid waste incinerator (MSWI) bottom ash in high calcium fly ash geopolymer matrix. Journal of Cleaner Production 148, 49–59. https://doi.org/10.1016/j.jclepro.2017.01.147

Zhang, B., Guo, H., Deng, L., Fan, W., Yu, T., Wang, Q., 2020a. Undehydrated kaolinite as materials for the preparation of geopolymer through phosphoric acid-activation. Applied Clay Science 199, 105887. https://doi.org/https://doi.org/10.1016/j.clay.2020.105887

Zhang, B., Guo, H., Yuan, P., Deng, L., Zhong, X., Li, Y., Wang, Q., Liu, D., 2020b. Novel

acid-based geopolymer synthesized from nanosized tubular halloysite: The role of precalcination temperature and phosphoric acid concentration. Cement and Concrete Composites 110, 103601. https://doi.org/https://doi.org/10.1016/j.cemconcomp.2020.103601

Zhang, B., Guo, H., Yuan, P., Li, Y., Wang, Q., Deng, L., Liu, D., 2020c. Geopolymerization of halloysite via alkali-activation: Dependence of microstructures on precalcination. Applied Clay Science 185, 105375. https://doi.org/https://doi.org/10.1016/j.clay.2019.105375

Zhu, W., Chen, X., Struble, L.J., Yang, E.H., 2018. Characterization of calcium-containing phases in alkali-activated municipal solid waste incineration bottom ash binder through chemical extraction and deconvoluted Fourier transform infrared spectra. Journal of Cleaner Production 192, 782–789. https://doi.org/10.1016/j.jclepro.2018.05.049

Table 1. Formulations of AACs using clay and WTS as precursors.

	(wt.% - wt.%)					
Clay - WTS	100 - 0	95 - 5	90 - 10	80 - 20	60 - 40	20 - 80
Reference	WTS-0	WTS-5	WTS-10	WTS-20	WTS-40	WTS-80

Table 2. Chemical composition (XRF) of clay and WTS used as precursors.

	SiO_2	Al_2O_3	Fe_2O_3	K_2O	TiO_2	CaO	MgO	MnO	P_2O_5	Na_2O	*LOI
Clay	59.87	22.87	6.33	1.38	1.04	0.73	0.61	0.02	0.06	0.32	6.09
WTS	28.25	15.72	3.10	2.16	0.45	10.65	2.04	0.80	0.80	0.29	34.72

*LOI: Loss of ignition at 1100ºC

Table 3. Chemical stability according to the boiling water test (Zhu et al., 2018; Davidovits, 2020).

WTS (wt.%)	Initial weight (g)	Final weight (g)	Loss (g)	Lost (%)	Result
0	11.587	-	-	-	Failure
5	11.107	10.399	0.708	6.37	Success
10	11.302	10.680	0.622	5.50	Success
20	11.544	11.168	0.376	3.26	Success
40	11.663	10.093	1.57	13.46	Failure
80	11.762	-	-	-	Failure

Table 4. Leaching test results following the EN 12457-4 standard ($mg \cdot kg^{-1}$).

	Clay	WTS	WTS-5	WTS-10	WTS-20	Inert	Non-hazardous	Hazardous
As	0.112	0.265	1.527	1.630	1.574	0.5	2	25
Ba	0.149	0.860	0.210	0.650	0.442	20	100	300
Cd	<0.001	<0.001	<0.001	<0.001	<0.001	0.04	1	5
Cr	0.025	0.013	0.975	0.983	0.839	0.5	10	70
Cu	0.150	0.080	0.542	0.757	1.318	2	50	100
Hg	<0.002	<0.005	<0.002	<0.002	<0.002	0.01	0.2	2
Mo	0.040	0.030	0.127	0.128	0.130	0.5	10	30
Ni	0.005	0.065	0.155	0.105	0.110	0.4	10	40
Pb	0.060	0.036	0.229	0.235	0.318	0.5	10	50
Se	0.022	<0.01	<0.02	<0.02	<0.02	0.1	0.5	7
Sb	0.011	<0.01	<0.01	<0.01	<0.01	0.06	0.7	5
Zn	0.052	0.173	0.875	0.952	1.201	4	50	200

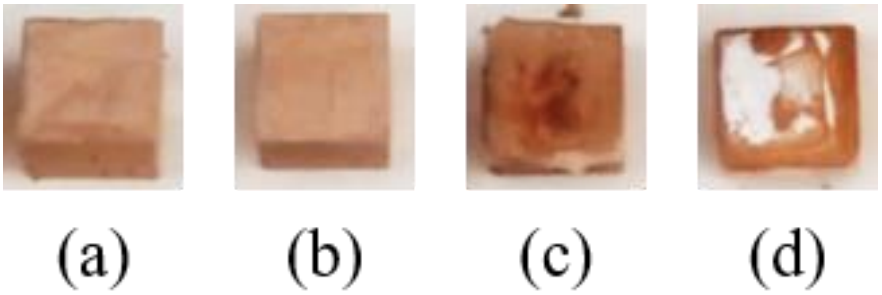

Fig.1. Cubic specimens (25x25x25 mm size) of clay AACs formulated with NaOH as activator (a) 2M, (b) 4M, (c) 8M and (d) 12M.

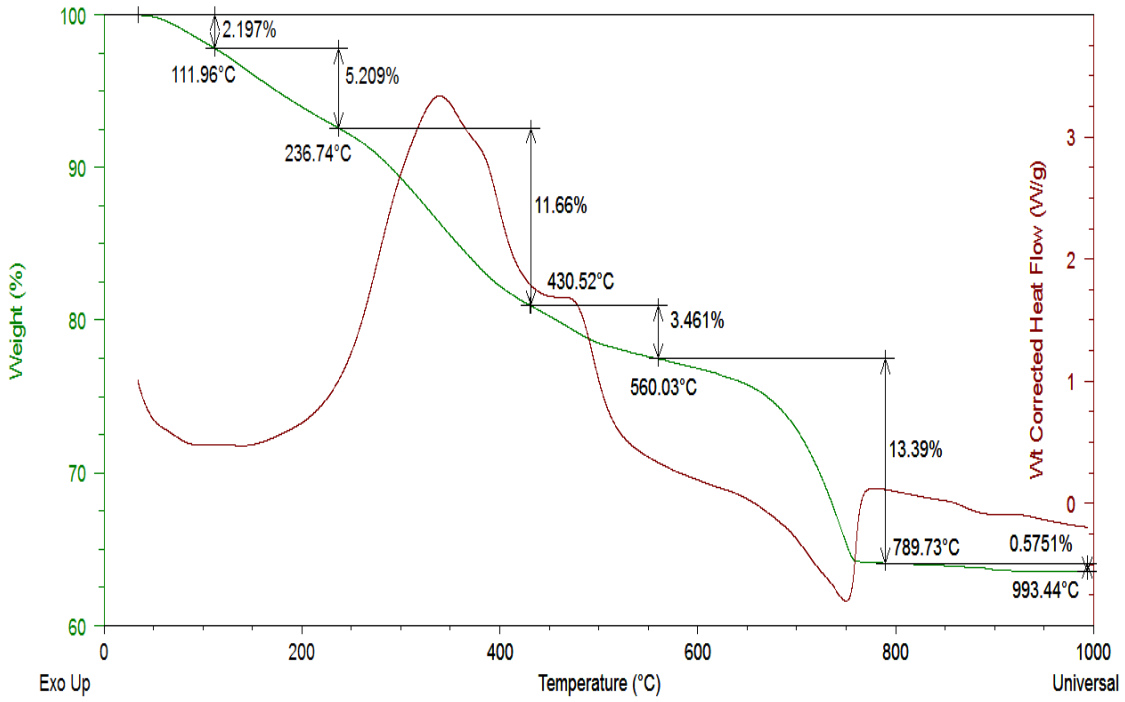

Fig. 2. TGA of WTS used as a precursor.

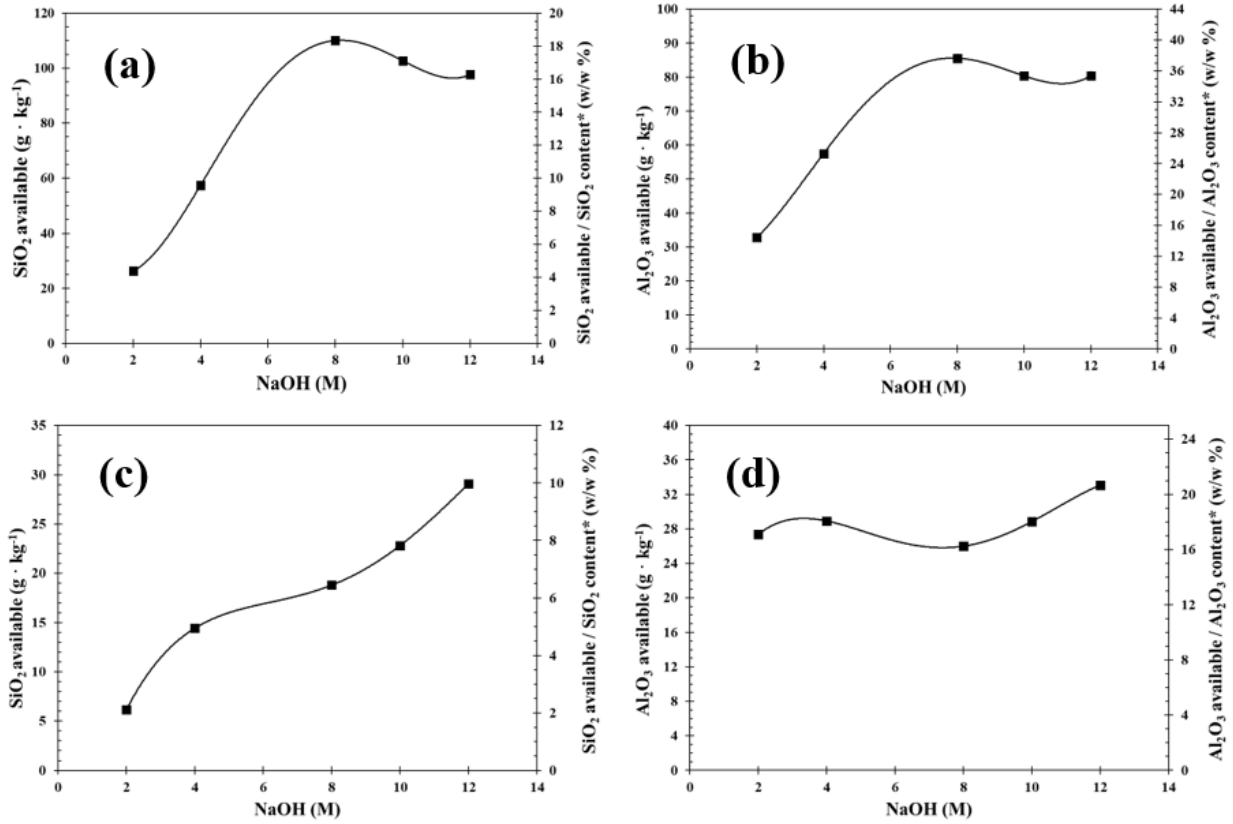

Fig. 3. Availability of SiO_2 and Al_2O_3 resulting from the chemical attacks of (a,b) clay and (c,d) WTS. *Results obtained from the XRF analysis (Table 2).

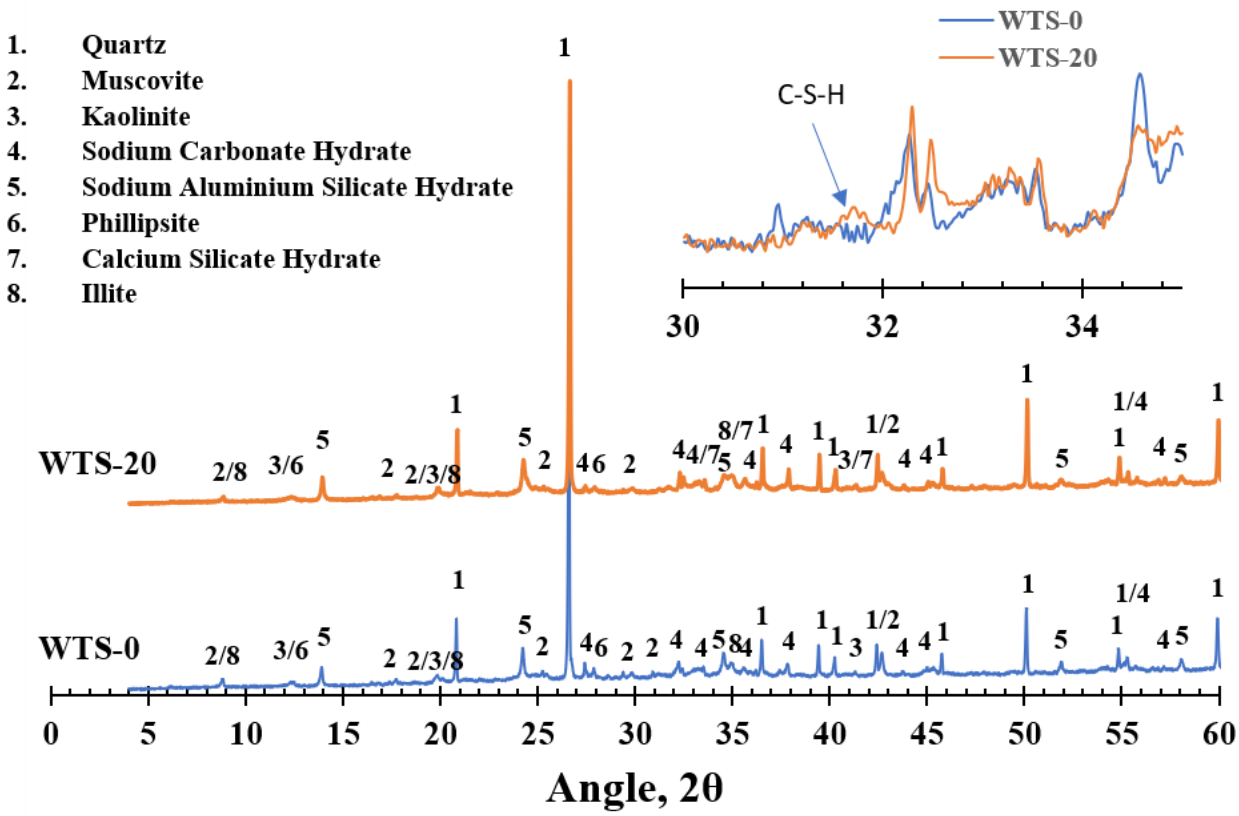

Fig.4. XRD diffractograms of WTS-0 and WTS-20 samples.

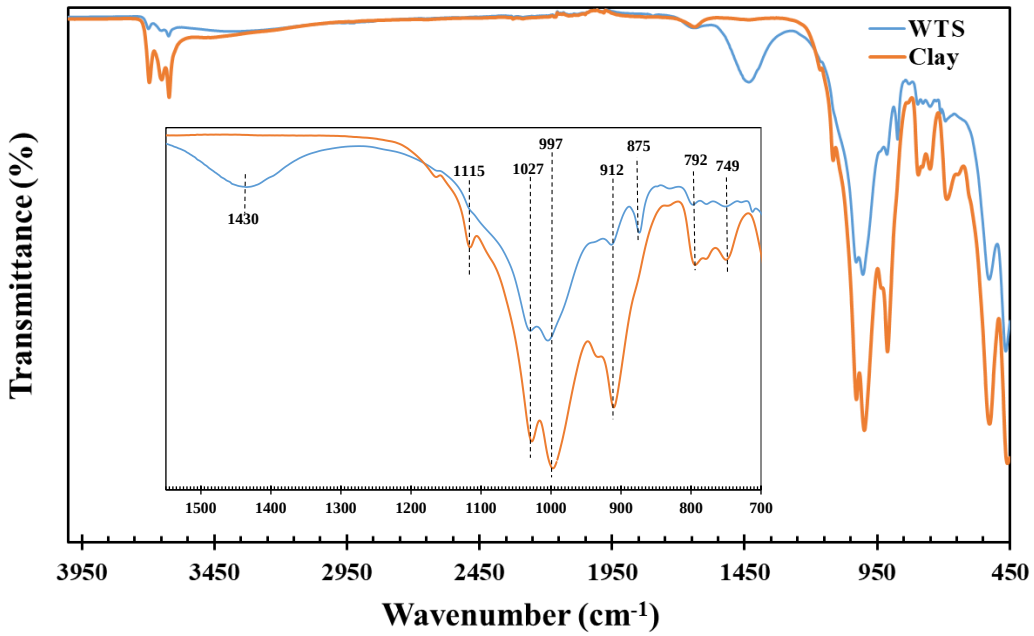

Fig. 5. FT-IR spectra of clay and WTS before the alkali activation.

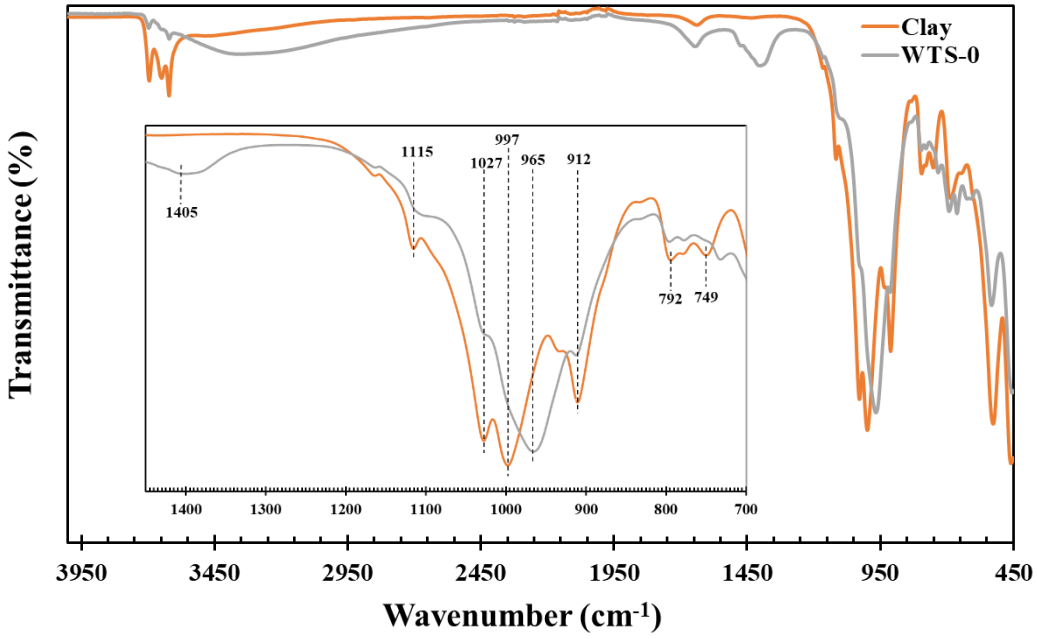

Fig. 6. FT-IR spectra of clay and WTS-0 samples.

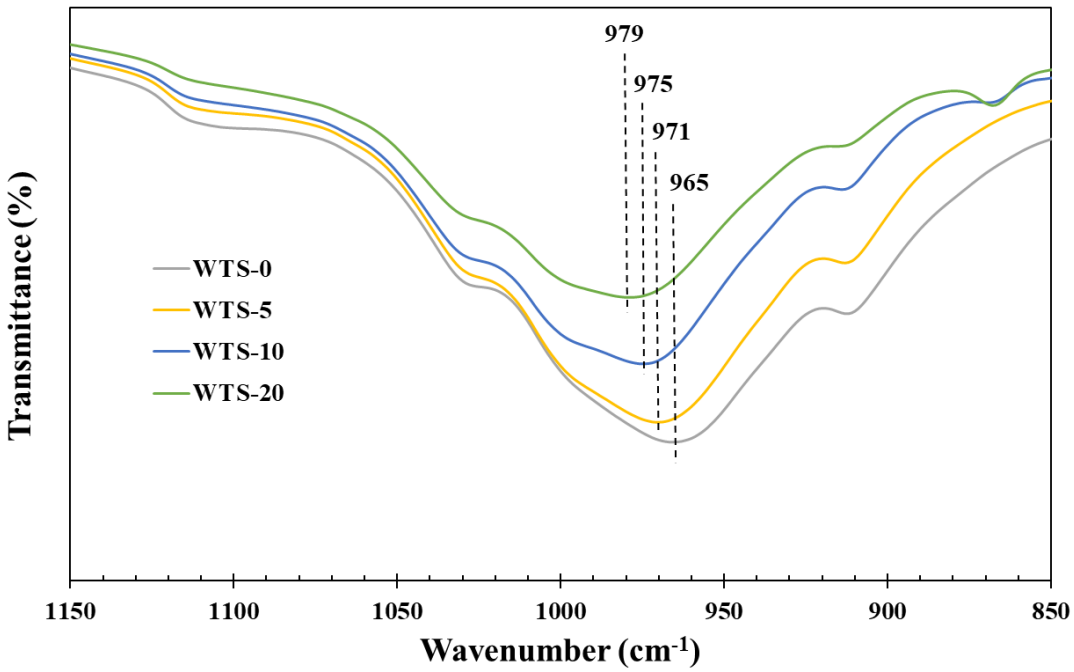

Fig. 7. FT-IR spectra of AAC where clay was replaced as precursor by different percentages (wt.%) of WTS.

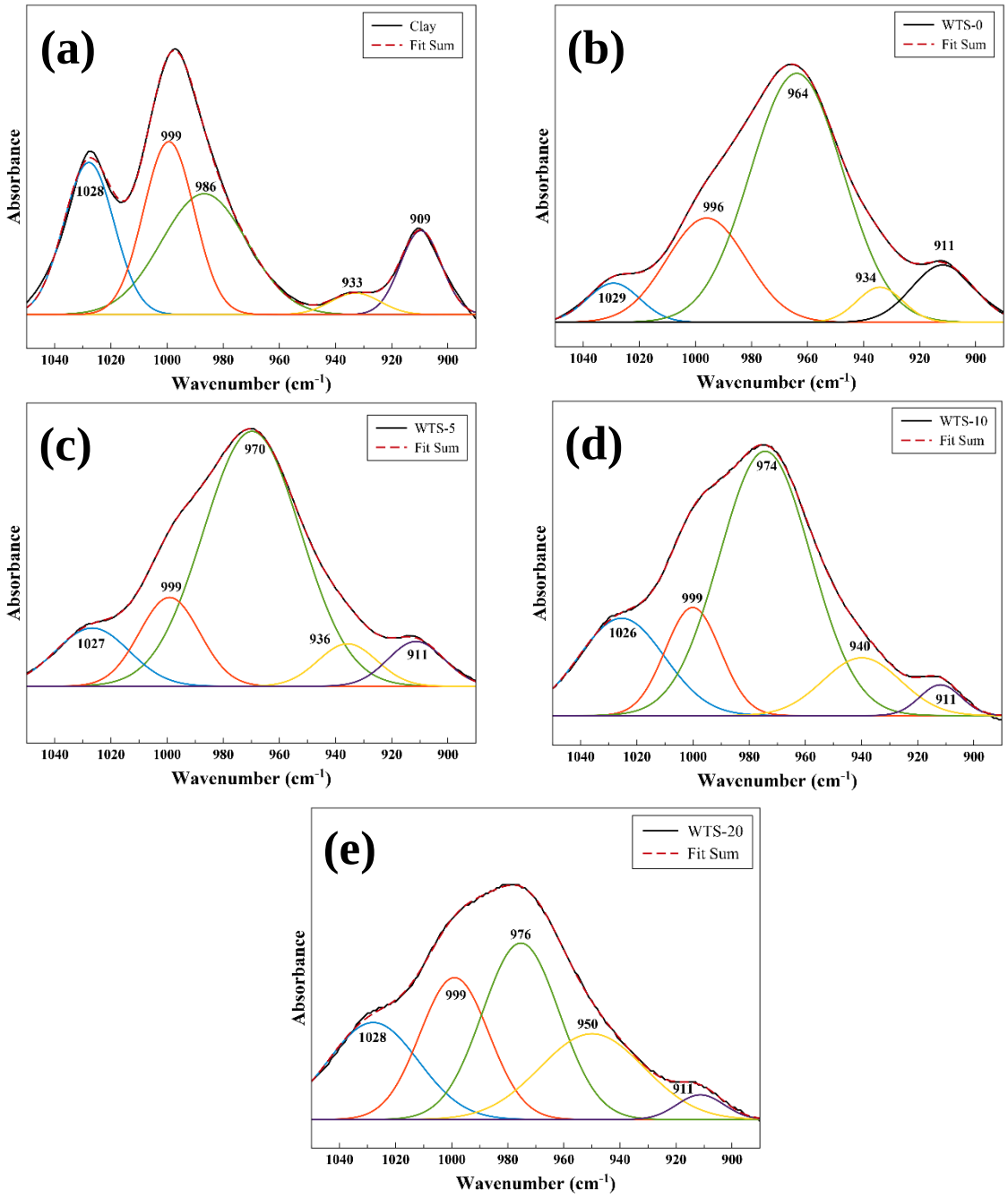

Fig 8. FT-IR spectral deconvolution of the midwavenumber region (1100 – 850 cm^{-1}) for (a) clay and (b) WTS-0, (c) WTS-5, (d) WTS-10 and (e) WTS-20 samples.

.

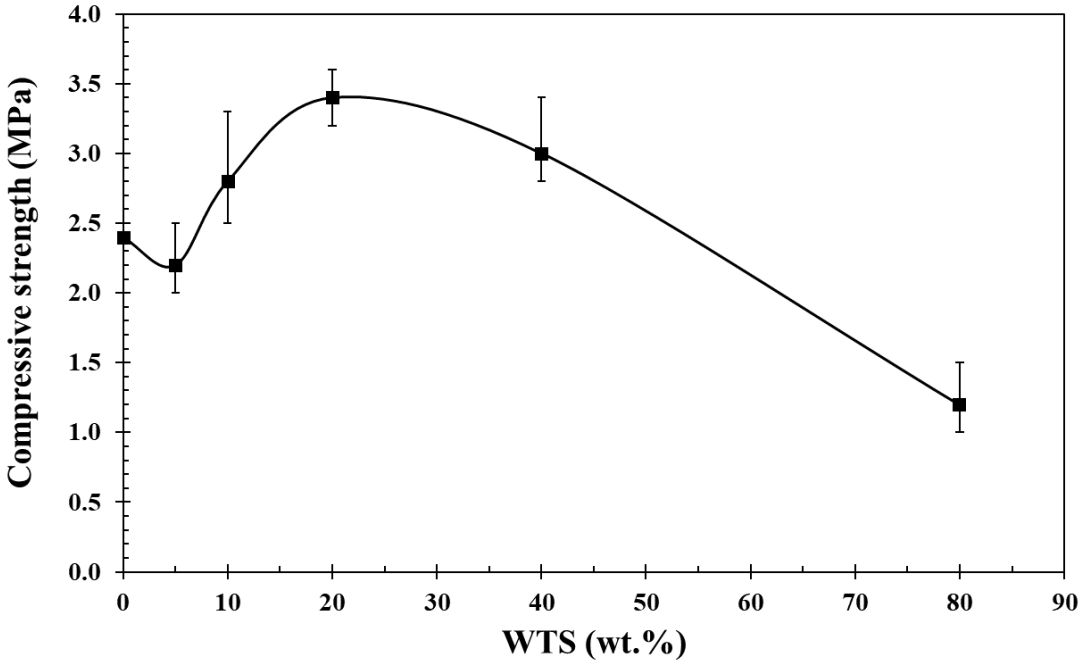

Fig. 9. Compressive strength (σ_c) of AAC specimens formulated using different percentage of WTS as precursor.